

The Effect of Pauli Operator on Nuclear Matter Properties within BHF Approach Using Argonne V_{18} Interaction

B. M. Elyan*, A. E. Elmeshneb, Kh. S. A. Hassaneen

Faculty of Science, Physics Department, Sohag University, Egypt

Abstract We have studied the equation of state (EOS) and the contribution of partial waves for symmetric nuclear matter (SNM) and pure neutron matter (PNM) to explain the effect of Pauli operator treatment. Our calculations have been carried out in the framework of Bruckner-Hartree-Fock (BHF) approach with angle average approximation and exact Pauli operator using Argonne V_{18} nucleon-nucleon interaction. From studying the partial waves contributions to the equation of state (EOS), we have explained the effect of the tensor force. The correct saturation point is still missed, so the considered model needs to a correction to be able to reproduce the empirical saturation point of symmetric nuclear matter.

Keywords BHF approach, Symmetric nuclear matter, Pure neutron matter, Angle average approximation, Exact Pauli operator, Single particle potential, Equation of state

1. Introduction

Different many body theories have been developed to understand the properties of the nuclear matter like the many body perturbation theory [1-5], the Monte Carlo method with its various versions [6-10], the variational method [11,12], and Bruckner-Hartree-Fock (BHF) approach [13,14].

BHF approach considers that the nucleons in nuclear matter move in a mean field arising from the interaction with all other nucleons (bound nuclear matter) and have overcome the difficulty of the treatment of the strong short-range repulsive core for the nucleon-nucleon (NN) interaction which makes nuclear system non-perturbative. Brueckner and others [15,16] developed the G-matrix method which called Brueckner-Bethe-Goldstone theory. The effect of the nuclear medium is taken into calculations via Pauli operator, which limits the allowed intermediate states above Fermi level and the denominator of the two body propagator contains the self energy.

The exact treatment of Pauli operator and of the energy denominator is essential for the calculations. The Pauli operator depends on the angles between the relative and the center of mass momenta of the two scattering nucleons besides the magnitude of them. This angular dependence makes a difficulty in the numerical computations due to the

coupling among the partial waves. Schiller [17] and others [18,19] have studied the exact treatment of Pauli operator. To avoid the coupling among the partial waves, the Pauli operator and the two nucleon energies averaged over the angle between the relative and the center of mass momenta. This is called angle average approximation [20,21].

One of the main aims of Brueckner-Bethe-Goldstone theory is to study the equation of state and reproduce the empirical saturation point. Tensor component of the NN interaction plays a central role in reproduction of the experimental phase shifts and responsible for the structure and the binding energy of the deuteron [22]. Discussing the effect of the tensor force on the equation of state is a main aim of this work as we will see below.

For both symmetric nuclear matter and pure neutron matter, we have carried out our calculations in the framework of BHF approach in three cases. The first case is by using the angle average approximation with the continuous choice of the single particle potential, the second by using the conventional one and the third is by using the exact Pauli operator.

BHF approach calculations depend on the choice of the single particle potential where the conventional choice considers a zero single particle energy above Fermi level [23], but the continuous choice assumes the self-consistent BHF potential extends above Fermi level, thus making the single particle potential a continuous function through the Fermi surface [24]. This continuous choice leads to an enhancement of correlation effects in the medium than the conventional one. The nucleon nucleon interaction employed in this work is Argonne V_{18} interaction [25].

* Corresponding author:

basma.elyan@yahoo.com (B. M. Elyan)

Received: Dec. 4, 2021; Accepted: Dec. 22, 2021; Published: Dec. 24, 2021

Published online at <http://journal.sapub.org/jnpp>

The Argonne V_{18} is non-relativistic potential defined in terms of local functions. It is with explicit charge dependence and charge symmetry. Wiringa *et al.* [25] have been updated Argonne V_{14} potential to fit both pp and np data with high quality. They added to the fourteen operators three additional charge-dependent and one charge-asymmetric operators. It called Argonne V_{18} and it gives a χ^2 per datum 1.09 for 4301 pp and nn data in the range 0-350 MeV. The nucleon nucleon Argonne V_{18} potential includes a complete electromagnetic part, one-pion-exchange (OPE) part and a short range phenomenological one.

2. The Theoretical Model

The main component of BHF approach is the G-matrix which is defined by the Bethe-Goldstone equation as:

$$G(\omega) = V + V \frac{Q}{\omega - H_o + i\eta} G(\omega) \quad (1)$$

where ω is the starting energy, V is the bare 2N potential, η is a small number, H_o is the unperturbed energy of the intermediate states and Q is the Pauli operator which projects out states with two nucleons above the Fermi level and it's donated by the relation:

$$Q(k, k') = (1 - \Theta_F(k))(1 - \Theta_F(k')) \quad (2)$$

where $\Theta_F(k) = 1$ for $k < k_F$ and zero otherwise and Θ_F is the occupation probability of a free Fermi gas with a Fermi momentum $k < k_F$.

According to BHF approach, the nuclear matter total energy is given by the expression:

$$E_A = \sum_k \frac{\hbar^2 k^2}{2m} + \frac{1}{2} \sum_{k' < k_F} \langle kk' | G(e(k) + e(k')) | kk' \rangle \quad (3)$$

where $|kk' \rangle$ refer to the anti-symmetrization of the G-matrix elements. The single particle energy $e(k)$ is the sum of the kinetic energy T and the single particle potential $U(k)$ and given by:

$$e(k) = T + U(k) = \frac{\hbar^2 k^2}{2m} + U(k) \quad (4)$$

where the $U(k)$ is given by the self-consistent equation according to eq. (3) as:

$$U(k) = \sum_{k' < k_F} \langle kk' | G(e(k) + e(k')) | kk' \rangle \quad (5)$$

The G-matrix can be used to determine the total energy per nucleon as follows:

In the case of the angle average of Pauli operator, the total energy per nucleon is given by:

$$E_A = \frac{3}{5} \frac{k_F^2}{2m} + \frac{6}{k_F^3} \sum_{T,S,I,J} (2T+1)(2J+1) \int_0^{k_F} dk k^2 \left[\int_0^{k_F-k} dK K^2 + \int_{k_F-k}^{k_F^2-k^2} dK K^2 \frac{k_F^2 - K^2 - k^2}{2Kk} \right] \langle klJ | G_{ST}(\omega, K) | klJ \rangle \quad (6)$$

where Ω is the angle between the direction of the relative momentum \vec{k} and the center of mass momentum \vec{K} .

And in the case of the exact of Pauli operator, it's given by:

$$E_A = \frac{3}{5} \frac{k_F^2}{2m} + \frac{6}{k_F^3} \sum_{\substack{T,S,M,I',I, \\ J',J,m_l,m_s}} (2T+1) \int k^2 dk \int K^2 dK \int d\Omega \times \langle klJ | G_{STM}(\omega, K) | kl'J' \rangle \quad (7)$$

$$(l'm_l m_s | J'M)(l m_l m_s | JM) Y_{l'm_l}(\Omega) Y_{l m_l}(\Omega)$$

$$\times \Theta(k_F - |\vec{K} + \vec{k}|) \Theta(k_F - |\vec{K} - \vec{k}|)$$

which corresponds to the standard expression discussed e.g. in [21].

By assuming a quadratic dependence of the single particle energy on the nucleon momentum, the single particle energy is written as:

$$e(k) = \begin{cases} \frac{\hbar^2 k^2}{2m} + \Delta & k \leq k_F \\ \frac{\hbar^2 k^2}{2m^*} & k > k_F \end{cases} \quad (8)$$

where m^* is the nucleon effective mass and Δ is a constant gives the single particle energy at $k=0$.

The nuclear incompressibility K is an important characteristic of the nuclear matter equation of state (EOS) and it's related to the curvature of the energy per nucleon E_A in symmetric nuclear matter around the saturation point by:

$$K = 9\rho^2 \frac{\delta^2(E_A)(\rho)}{\delta\rho^2} \Big|_{\rho=\rho_0} \quad (9)$$

3. Results and Discussion

3.1. Single Particle Potential

The single particle energy was represented by Eq. (4) as the sum of the kinetic energy T and the single particle potential $U(k)$. As long as the kinetic energy is independent of the method of calculation, we will restrict our discussion on the single particle potential.

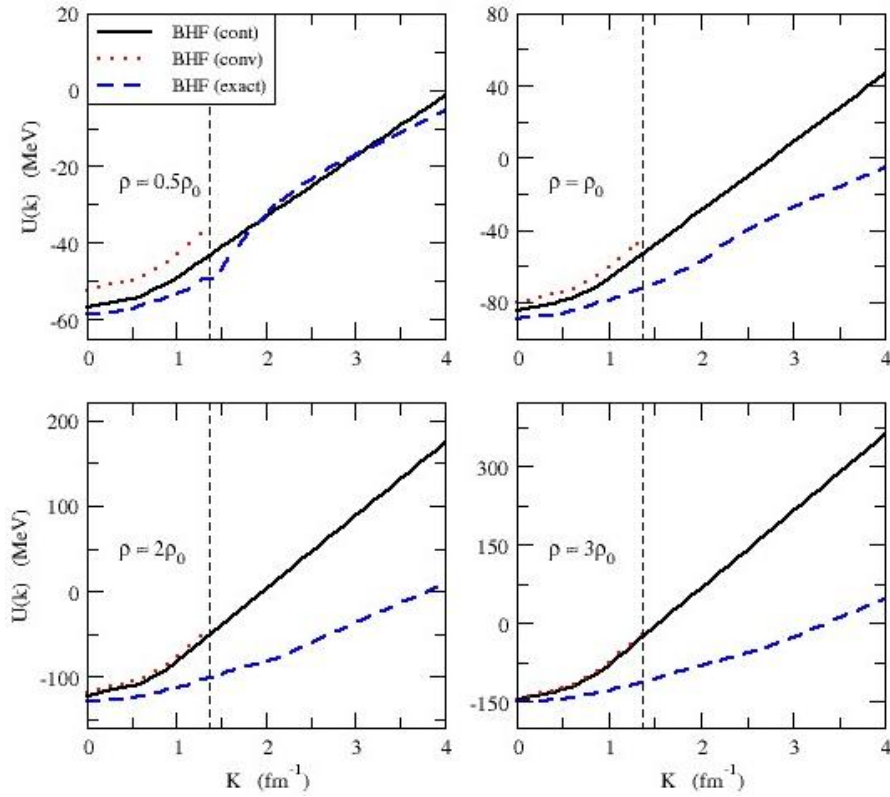


Figure 1. The single particle potential $U(k)$ as a function of momentum k at different densities using Argonne V_{18} potential for symmetric nuclear matter

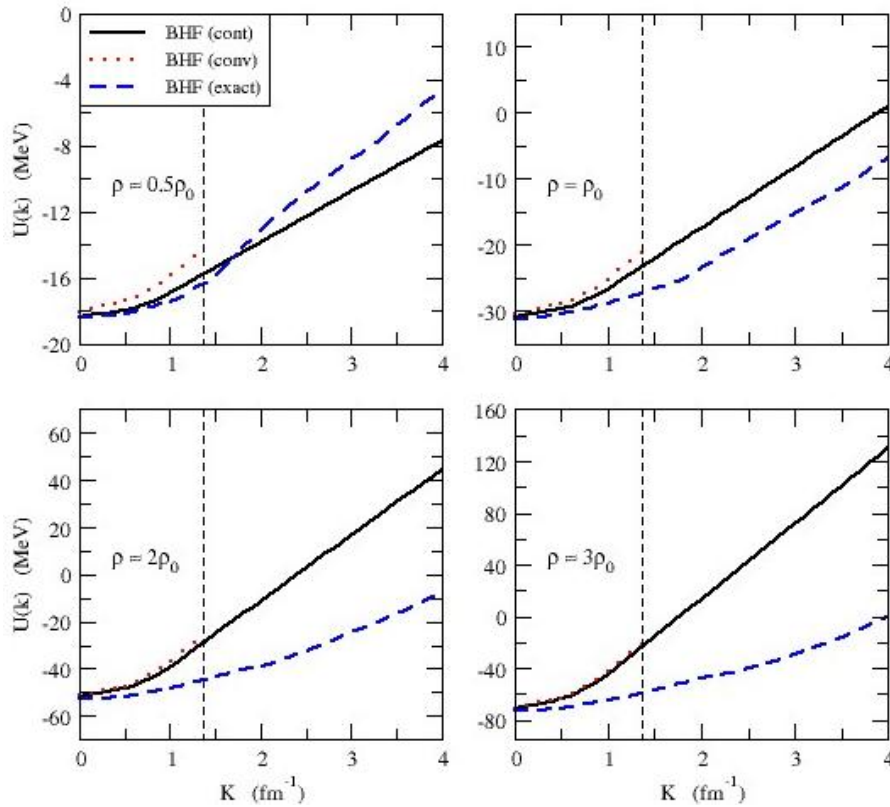


Figure 2. The single particle potential $U(k)$ as a function of momentum k at different densities using Argonne V_{18} potential for pure neutron matter

In this work we have calculated the single particle potential $U(k)$ for symmetric nuclear matter and pure neutron matter according to eq.(5) using Argonne V_{18} potential. The calculations have carried out with angle average approximation and exact Pauli operator. We plot the dependence of the single particle potential $U(k)$ on the momentum k at different densities ($\rho \approx 0.5\rho_0$, ρ_0 , $2\rho_0$ and $3\rho_0$, where ρ_0 is the saturation density) in figs. (1) and (2) for the considered potential. The dotted curve represents the conventional choice which assumes a zero single particle potential for single-particle states above the Fermi level and U is self-consistent BHF potential for $k < k_F$ [26], the solid one represents the continuous choice for which the self-consistency of the BHF potential extends to $k > k_F$, and the dashed one represents exact Pauli operator. We notice that $U(k)$ has a simple parabolic shape, increases with increasing k and the curve that represents the conventional choice is more repulsive than the other curves.

Table 1. The potential depth values at different densities for Argonne V_{18}

Model	Potential depth (MeV)			
	at $\rho \approx 0.5\rho_0$	at $\rho = \rho_0$	at $\rho \approx 2\rho_0$	at $\rho \approx 3\rho_0$
	SNM			
BHF with angle average approx. (cont)	-56.8659	-84.7308	-122.103	-147.518
BHF with angle average approx. (conv)	-52.4979	-80.1611	-118.004	-145.016
BHF with exact Pauli operator	-58.7875	-88.9538	-128.359	-149.136
PNM				
BHF with angle average approx. (cont)	-18.4143	-31.0003	-52.0838	-71.753
BHF with angle average approx. (conv)	-18.0509	-30.5872	-51.4876	-71.2059
BHF with exact Pauli operator	-18.4457	-31.2009	-52.832	-72.9062

The values of the potential depth which represents the value of $U(k)$ at $k=0$ are listed in table (1) for symmetric nuclear matter and pure neutron matter. We notice that the potential depth decreases with increasing density. Also, it is more repulsive in the angle average approximation than the exact Pauli operator. That reflects the fact that the effective interaction is more attractive between nucleons in the exact Pauli operator than the angle average approximation [27]. When the density increases, the values of the single particle potential becomes more attractive at low momentum, and more repulsive at high momentum. Also, the difference between the values for the continuous choice and the conventional one decreases (the

curves converge from each other), but the difference between the values for the angle average approximation and the exact Pauli operator increases (the curves diverge from each other).

By comparing fig. (1) and fig. (2) we notice that the values of the single particle potential in symmetric nuclear matter at low momenta are more attractive than that of pure neutron matter, due to the absence of the ${}^3S_1 - {}^3D_1$ which increase the attraction. But at high momenta, the values of the single particle potential in symmetric nuclear matter more repulsive than that of pure neutron matter.

3.2. Partial Waves Contribution

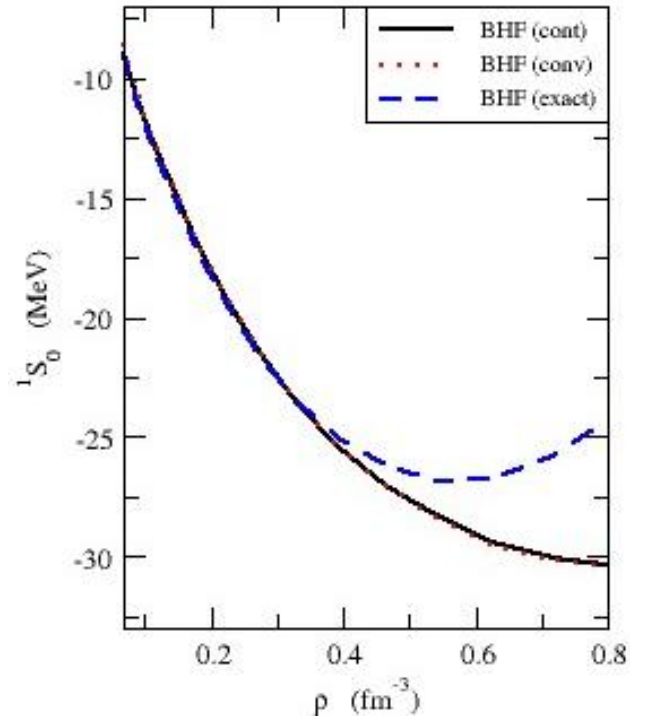


Figure 3. The 1S_0 partial wave as a function of density ρ using Argonne V_{18} potential for symmetric nuclear matter

In this section, we will discuss the potential energy per nucleon originating from various partial waves up to $J=9$, where the contribution coming from higher partial waves is negligible. This contribution of the partial waves have studied using angle average approximation and exact Pauli operator without adding any correlations. The calculation carried out for symmetric nuclear matter and pure neutron matter using Argonne V_{18} potential.

Figs. (3) and (4) show the 1S_0 partial wave as a function of density ρ for symmetric nuclear matter and pure neutron matter, respectively. The value of 1S_0 component in the three cases, the continuous choice (bold curve), the conventional one (dotted curve), and the exact Pauli operator (dashed curve) decreases with increasing density. But in the cases of exact Pauli operator, it decreases until reaches a minimum value then increases with

increasing density. The curve that represents the exact Pauli operator is more repulsive than others, and this means the exact treatment of Pauli operator makes a significant change by inducing a substantial repulsion with increasing density.

Fig. (5) displays the ${}^3S_1-{}^3D_1$ partial wave as a function of density ρ for symmetric nuclear matter in the above mentioned cases. This partial wave takes negative values only, therefore it's responsible for the bound state of the symmetric nuclear matter. This clarifies the absence of this component for pure neutron matter. The three cases have the same behavior, the ${}^3S_1-{}^3D_1$ component value decreases with increasing density until reaches a minimum value then increases with increasing density. In the same figure we notice that the curve which represents the exact Pauli operator is more attractive at small densities than others, this is due to the enhancement of the tensor force. Tensor force is a very important source for the origin of the two-body correlations and originally is in a relative 3S_1 state with momentum below k_F into a 3D_1 state above k_F [27]. The measure of tensor force is called D-state probability P_D obtained for the deuteron, which equals 5.76% for Argonne V_{18} [28]. This large value of D-state probability for Argonne V_{18} comparing with that for other NN interactions refers to the strong tensor force for Argonne V_{18} [29].

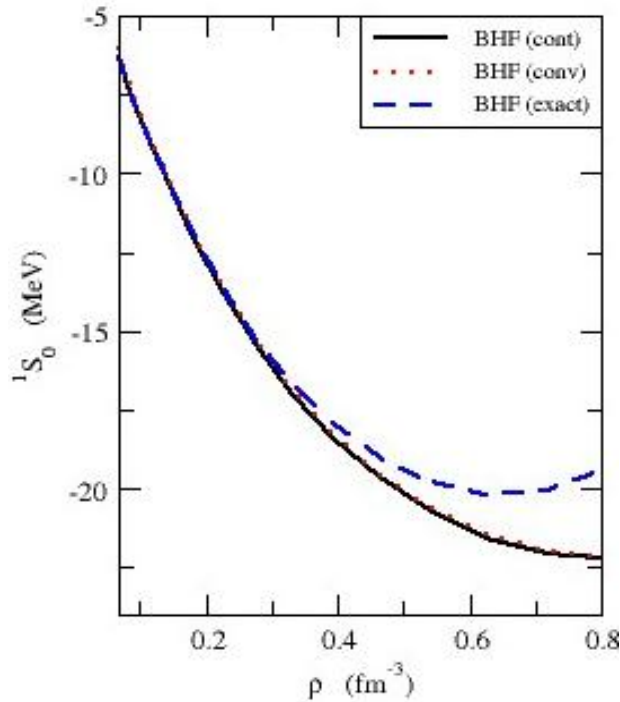


Figure 4. The 1S_0 partial wave as a function of density ρ using Argonne V_{18} potential for pure neutron matter

Figs. (6) and (7) show the 3P_0 partial wave as a function of density ρ for symmetric nuclear matter and

pure neutron matter, respectively. It's value decreases with increasing density until reaches a minimum value then increases with increasing density. The effect of the exact treatment is large at high densities, especially for pure neutron matter.

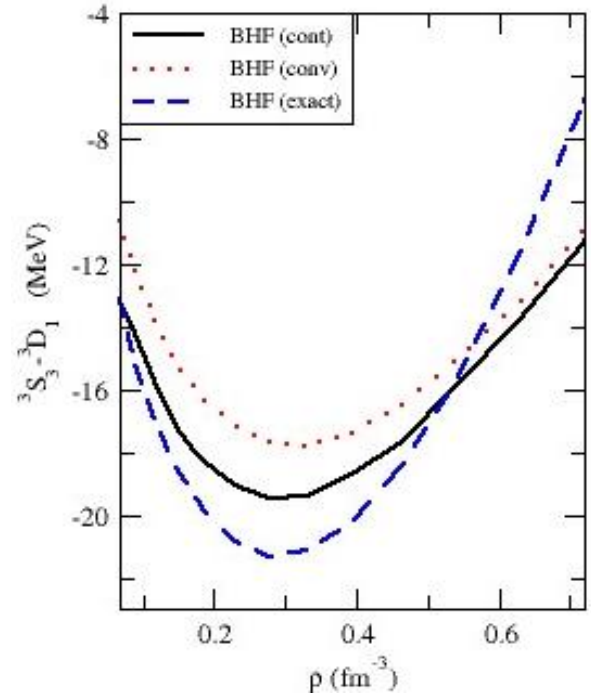


Figure 5. The ${}^3S_1-{}^3D_1$ partial wave as a function of using Argonne V_{18} potential for symmetric nuclear matter

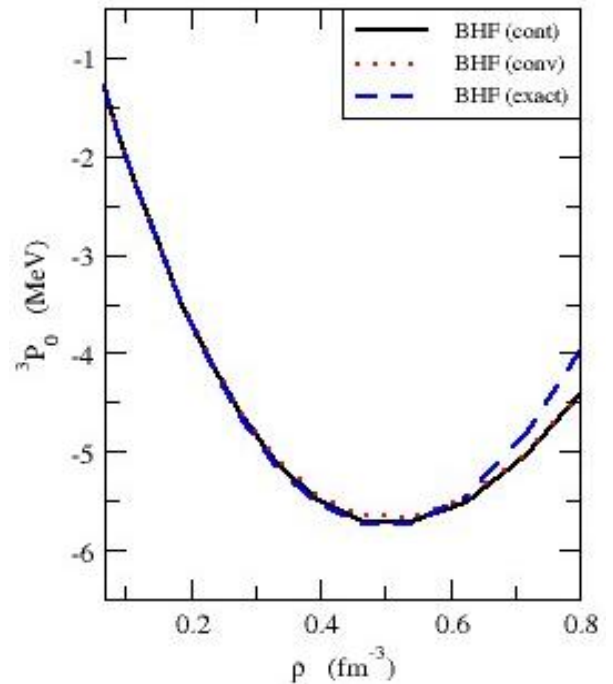


Figure 6. The 3P_0 partial wave as a function of density ρ using Argonne V_{18} potential for symmetric nuclear matter

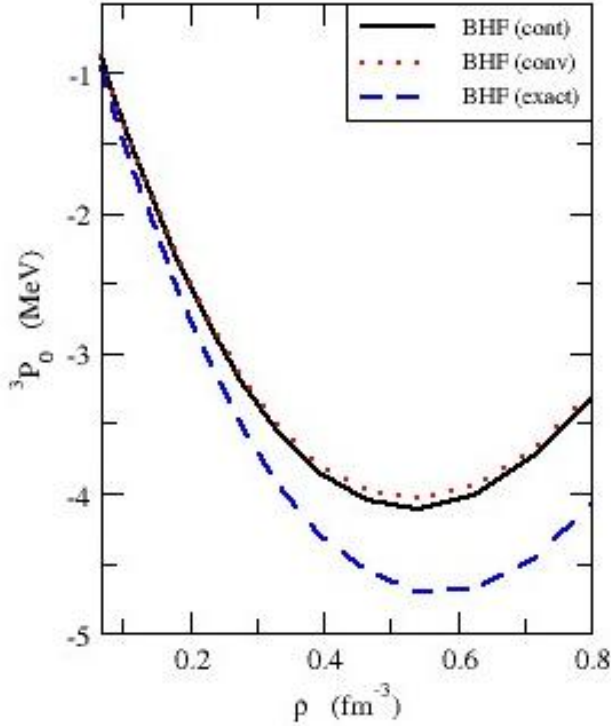


Figure 7. The 3P_0 partial wave as a function of density ρ using Argonne V_{18} potential for pure neutron matter

Table 2. Partial waves for symmetric nuclear matter using Argonne V_{18}

Partial wave	Cont	Conv	Exact
1S_0	-16.3397	-16.2794	-16.6014609
${}^3S_1-{}^3D_1$	-17.9279	-15.9059	-19.3577653
3P_0	-3.2222	-3.2065	-3.23344636
3P_1	9.6989	9.9744	9.59325122
1P_1	3.87	3.9413	3.86152867
1D_2	-2.575	-2.5593	-2.62137626
3D_2	-3.8888	-3.8305	-3.97487678
${}^3P_2-{}^3F_2$	-7.8829	-7.647	-7.97204746
1F_3	0.7437	0.7448	0.797261692
3F_3	1.2535	1.2547	1.31402458
1G_4	-0.3492	-0.3490	-0.396416063
3G_4	-0.6280	-0.6262	-0.709202212
${}^3D_3-3G_3$	0.1294	0.1827	0.107606517
${}^3F_4-3H_4$	-0.3936	-0.3895	-0.400250776
Total potential energy	-37.5118	-34.6954	-39.1934

Table (2) displays the partial waves contributions for symmetric nuclear matter using angle average approximation with his two choices and exact Pauli operator at the saturation density $\rho_s = 0.17m^{-3}$. Table (3) is the sam as (2) but for pure neutron matter. From this table, we can say 1S_0 and ${}^3S_1-{}^3D_1$ partials waves are more important than other partial waves and have the main contribution to EOS.

Table 3. Partial waves for pure neutron matter using Argonne V_{18}

Partial wave	Cont	Conv	Exact
1S_0	-11.5413	-11.4103	-11.4808796
3P_0	-2.1997	-2.1836	-2.39486525
3P_1	6.2478	6.421	6.47987034
1D_2	-1.7255	-1.7143	-1.84386604
${}^3P_2-{}^3F_2$	-5.4457	-5.2686	-5.69295134
3F_3	0.8351	0.8360	0.997527605
1G_4	-0.2329	-0.2327	-0.30121265
${}^3F_4-3H_4$	-0.265	-0.2622	-0.307601558
Total potential energy	-14.3272	-13.8147	-14.3835

3.3. Equation of State

The results of EOS calculations are plotted in fig. (8) for symmetric nuclear matter. The dotted curve represents the conventional choice, the solid one represents the continuous choice, and the dashed one represents the exact Pauli operator. The empirical saturation point indicated by square box, whereas the solid points refer to the calculated saturation points.

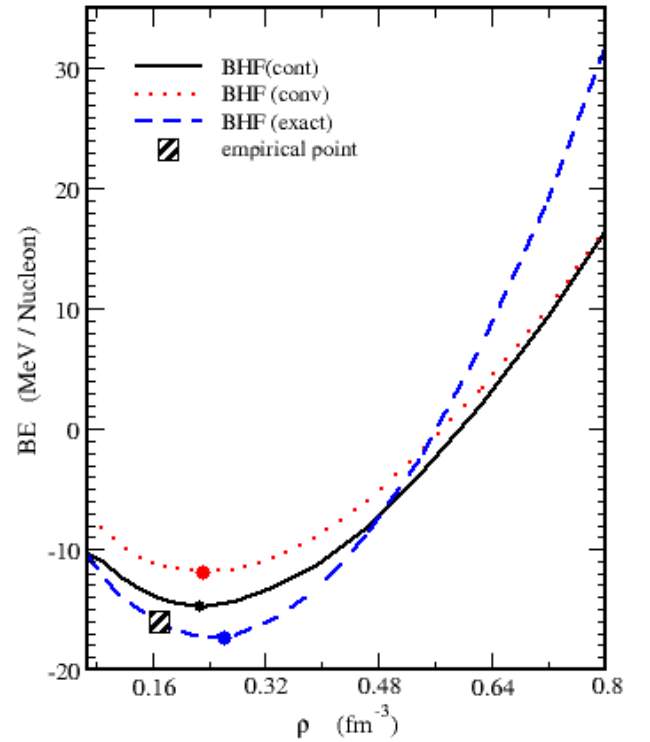


Figure 8. The binding energy per nucleon E/A as a function of density ρ using Argonne V_{18} potential for symmetric nuclear matter

One notice from this figure that the binding energy per nucleon decreases at first with increasing density ρ until reaches the saturation point, then it increases with increasing density ρ . The binding energy per particle E_A using Argonne V_{18} takes repulsive values. This means that the quenching effect, which reduces the interaction of non-Born terms in the G-matrix efficient for Argonne V_{18} ,

consequently Argonne V_{18} potential yield more repulsion compared to other potentials [27]. The curve that represents the exact treatment of Pauli operator is more attractive than other curves at low densities but is more repulsive at high densities. Table (4) shows the saturation points in the three cases for the considered potential. The saturation points are fallen on a band (called Coester band [30]) shifted with respect to the empirical saturation point ($\rho_0 = 0.17 \text{ fm}^{-3}; E_A = -16 \text{ MeV}$).

It's obvious that the saturation point in case of the exact treatment of Pauli operator and the continuous choice is closer to the empirical point than the conventional one. Therefore, the exact treatment of Pauli operator and the continuous choice lead to an enhancement of correlation effects and the exact treatment of Pauli operator predicts larger binding energy for nuclear matter.

Fig. (9) shows the EOS results for pure neutron matter. The binding energy per nucleon takes positive values only which increases rapidly with increasing density. It's clear that the effect of exact treatment of Pauli operator is negligible.

The empirical value of the incompressibility for symmetric nuclear matter (SNM) at the saturation density ρ_0 is $230 \pm 40 \text{ MeV}$ [43]. The calculated values of K according to equation (9) for the considered cases using Argonne V_{18} are listed in table (4). We observe that the value of K in the case of exact Pauli operator lies on the range of the experimental measurement. This refers to the good effect of the exact treatment of Pauli operator. A comparison of our nuclear matter binding energy, saturation density as well as incompressibility with other many-body methods for various potentials is also listed in table (4).

It can be seen from this table that our results for the EOS and that for other approaches for the same NN interaction are different due to the difference of the theoretical treatment in every approach. But our results in the case of BHF with exact Pauli operator is the best, because it's closer to the empirical result.

The importance of determining the value of incompressibility arises from its impact on the physics of supernovae and neutron stars.

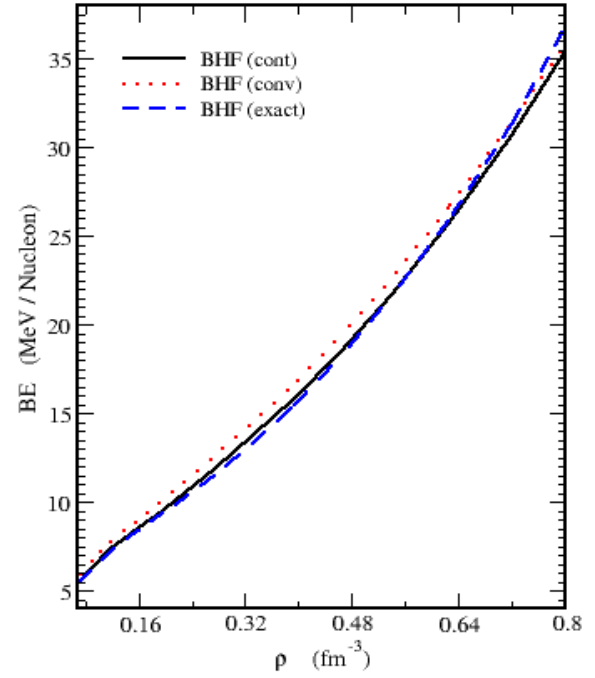


Figure 9. The binding energy per nucleon E/A as a function of density ρ using Argonne V_{18} potential for pure neutron matter

Table 4. A comparison of the obtained saturation properties of nuclear matter with several many-body interactions and techniques

Potential	Method	Author	$\rho_0 (\text{fm}^{-3})$	$EA (\text{MeV})$	$K (\text{MeV})$
Reid 93	LOCV	MM [31]	0.48	-32.07	–
Reid 93	BHF	LLSZCM [32]	0.328	-19.8	–
AV_{14}	BHF	LLSZCM [32]	0.276	-18.1	–
AV_{14}	LOCV	HZMG [33]	0.33	-22.7	354
AV_{14}	RLOCV	HZMG [33]	0.37	-24.9	316
AV_{14}	VHC	WFF [34]	0.32	-15.6	205
Bonn C	DBHF	KS [36]	0.48	-14.14	170
Paris	VHC	T [37]	0.2	-15.2	145
Paris	BHF	LLSZCM [32]	0.27	-17.6	–
Nijmegen	BHF	RSPHG [38]	0.28	-18.78	–
Nijmegen	Tmatrix	SB [39]	0.235	-18.4	76
Nijmegen	BHF	LLSZCM [32]	0.348	-20.7	–
AV_{18}	LOCV	GM [40]	0.327	23.37	373.3
AV_{18}	VHC	APR [42]	0.3	-18.22	289
AV_{18}	BHF AA (cont)	This work	0.2270	-14.7952	139.9081
AV_{18}	BHF AA (conv)	This work	0.2309	-11.9022	119.3848
AV_{18}	BHF (exact)	This work	0.2613	-17.3072	211.0284
Empirical	–	–	0.17 ± 0.01	-16	230 ± 40

4. Conclusions

From the above mentioned, we would like to show that the exact treatment of Pauli operator has a good enhancement in medium better than the angle average approximation. Tensor force effect appears by introducing the partial waves contributions, especially the 3S_1 – 3D_1 partial wave. The presence of 3S_1 – 3D_1 partial wave in symmetric nuclear matter (SNM) and its absence in pure neutron matter (PNM) interpreted the unbound state for pure neutron matter (PNM).

By using the exact treatment of Pauli operator, we have obtained a correct value of the incompressibility. But the effect of this treatment is not a very large around the empirical saturation point at small densities. Comparing our results with previous studies, we found that empirical saturation point is missed and we must add a correction to the present model to obtain the correct saturation point. This correction may be the three body forces which makes the results more repulsive.

REFERENCES

- [1] K. Hebeler, S. K. Bogner, R. J. Furnstahl, A. Nogga, and A. Schwenk. Improved nuclear matter calculations from chiral low-momentum interactions. *Phys. Rev. C*, 83:031301, Mar 2011.
- [2] I. Tews, T. Krüger, K. Hebeler, and A. Schwenk. Neutron matter at next-to-next-to-next-to-leading order in chiral effective field theory. *Phys. Rev. Lett.*, 110:032504, Jan 2013.
- [3] Jeremy W. Holt, Norbert Kaiser, and Wolfram Weise. Nuclear chiral dynamics and thermodynamics. *Progress in Particle and Nuclear Physics*, 73:35–83, 2013.
- [4] Corbinian Wellenhofer, Jeremy W. Holt, and Norbert Kaiser. Thermodynamics of isospin-asymmetric nuclear matter from chiral effective field theory. *Phys. Rev. C*, 92:015801, Jul 2015.
- [5] C. Drischler, K. Hebeler, and A. Schwenk. Chiral interactions up to next-to-next-to-next-to-leading order and nuclear saturation. *Phys. Rev. Lett.*, 122:042501, Jan 2019.
- [6] B. S. Pudliner, V. R. Pandharipande, J. Carlson, and R. B. Wiringa. Quantum monte carlo calculations of $A \leq 6$ nuclei. *Phys. Rev. Lett.*, 74:4396 – 4399, May 1995.
- [7] K.E. Schmidt and S. Fantoni. A quantum monte carlo method for nucleon systems. *Physics Letters B*, 446(2): 99–103, 1999.
- [8] Steven C. Pieper and R. B. Wiringa. Quantum monte carlo calculations of light nuclei. *Annual Review of Nuclear and Particle Science*, 51(1):53–90, 2001.
- [9] J. Carlson, J. Morales, V. R. Pandharipande, and D. G. Ravenhall. Quantum monte carlo calculations of neutron matter. *Phys. Rev. C*, 68:025802, Aug 2003.
- [10] Alexandros Gezerlis and J. Carlson. Low-density neutron matter. *Phys. Rev. C*, 81:025803, Feb 2010.
- [11] V. R. Pandharipande and R. B. Wiringa. Variations on a theme of nuclear matter. *Rev. Mod. Phys.*, 51:821–861, Oct 1979.
- [12] F. Arias de Saavedra, C. Bisconti, G. Co’, and A. Fabrocini. Renormalized fermi hyper-netted chain approach in medium-heavy nuclei. *Physics Reports*, 450(1):1–95, 2007.
- [13] K. A. Brueckner, C. A. Levinson, and H. M. Mahmoud. Two-body forces and nuclear saturation. i. central forces. *Phys. Rev.*, 95:217–228, Jul 1954.
- [14] K. A. Brueckner. Many-body problem for strongly interacting particles. ii. linked cluster expansion. *Phys. Rev.*, 100:36–45, Oct 1955.
- [15] J. Goldstone. Derivation of the Brueckner Many-Body Theory. *Proc. Roy. Soc. Lond. A*, 239:267–279, 1957.
- [16] H. A. Bethe, B. H. Brandow, and A. G. Petschek. Reference spectrum method for nuclear matter. *Phys. Rev.*, 129:225–264, Jan 1963.
- [17] E. Schiller, H. Müther, and P. Czerski. Pauli exclusion operator and binding energy of nuclear matter. *Phys. Rev. C*, 59:2934–2936, May 1999.
- [18] K. Suzuki, R. Okamoto, M. Kohno, and S. Nagata. Exact treatment of the pauli exclusion operator in nuclear matter calculation. *Nuclear Physics A*, 665(1):92–104, 2000.
- [19] F. Sammarruca, X. Meng, and E. J. Stephenson. Exact treatment of the pauli exclusion operator in nuclear matter. *Phys. Rev. C*, 62:014614, Jun 2000.
- [20] K. A. Brueckner and J. L. Gammel. Properties of nuclear matter. *Phys. Rev.*, 109:1023– 1039, Feb 1958.
- [21] Michael I. Haftel and Frank Tabakin. Nuclear saturation and the smoothness of nucleon-nucleon potentials. *Nuclear Physics A*, 158(1):1 – 42, 1970.
- [22] Arianna Carbone, Artur Polls, and Arnau Rios. Symmetric nuclear matter with chiral three-nucleon forces in the self-consistent green’s functions approach. *Phys. Rev. C*, 88:044302, Oct 2013.
- [23] H. Kümmel, K.H. Lührmann, and J.G. Zabolitzky. Many-fermion theory in exs- (or coupled cluster) form. *Physics Reports*, 36(1):1 – 63, 1978.
- [24] J.P. Jeukenne, A Lejeune, and C Mahaux. Many-body theory of nuclear matter. *Physics Reports*, 25(2):83–174, 1976.
- [25] R. B. Wiringa, V. G. J. Stoks, and R. Schiavilla. Accurate nucleon-nucleon potential with charge-independence breaking. *Phys. Rev. C*, 51:38–51, Jan 1995.
- [26] H Müther and A Polls. Two-body correlations in nuclear systems. *Progress in Particle and Nuclear Physics*, 45(1): 243 – 334, 2000.
- [27] Kh.S.A. Hassaneen, H.M. Abo-Elsebaa, E.A. Sultan, and H.M.M. Mansour. Nuclear binding energy and symmetry energy of nuclear matter with modern nucleon–nucleon potentials. *Annals of Physics*, 326(3): 566 – 577, 2011.
- [28] B. D. Day. Nuclear saturation from two-nucleon potentials.

- Phys. Rev. Lett., 47:226–229, Jul 1981.
- [29] Morten Hjorth-Jensen, Thomas T.S. Kuo, and Eivind Osnes. Realistic effective interactions for nuclear systems. *Physics Reports*, 261(3):125–270, 1995.
- [30] F. Coester, S. Cohen, B. Day, and C. M. Vincent. Variation in nuclear-matter binding energies with phase-shift-equivalent two-body potentials. *Phys. Rev. C*, 1:769–776, Mar 1970.
- [31] G H Bordbar and M Modarres. LOCV calculation of nuclear matter with phenomenological two-nucleon interaction operators. *Journal of Physics G: Nuclear and Particle Physics*, 23(11): 1631–1646, nov 1997.
- [32] Z. H. Li, U. Lombardo, H.-J. Schulze, W. Zuo, L. W. Chen, and H. R. Ma. Nuclear matter saturation point and symmetry energy with modern nucleon-nucleon potentials. *Phys. Rev. C*, 74:047304, Oct 2006.
- [33] S. Heidari, S. Zaryouni, H. R. Moshfegh, and S. Goudarzi. Role of relativistic effects and three-body forces in nuclear matter properties. *Phys. Rev. C*, 99:024307, Feb 2019.
- [34] R. B. Wiringa, V. Fiks, and A. Fabrocini. Equation of state for dense nucleon matter. *Phys. Rev. C*, 38:1010–1037, Aug 1988.
- [35] E.N.E. van Dalen, C. Fuchs, and Amand Faessler. The relativistic dirac–brueckner approach to asymmetric nuclear matter. *Nuclear Physics A*, 744:227–248, Nov 2004.
- [36] Tetsuya Katayama and Koichi Saito. Properties of dense, asymmetric nuclear matter in dirac-brueckner-hartree-fock approach. *Physical Review C*, 88(3): 035805, 2013.
- [37] Masatoshi Takano. Variational method for infinite nuclear matter with the paris potential. *Progress of Theoretical Physics*, 104(1): 185–202, 2000.
- [38] Syed Rafi, Manjari Sharma, Dipti Pachouri, W Haider, and YK Gambhir. Equation of state and the nucleon optical potential with three-body forces. *Physical Review C*, 87(1): 014003, 2013.
- [39] V. Somà and P. Božek. In-medium t matrix for nuclear matter with three-body forces: Binding energy and single-particle properties. *Phys. Rev. C*, 78: 054003, Nov 2008.
- [40] S. Goudarzi and H. R. Moshfegh. Effects of three-body forces on the maximum mass of neutron stars in the lowest-order constrained variational formalism. *Phys. Rev. C*, 91:054320, May 2015.
- [41] Isaac Vidaña, Constan ça Providência, Artur Polls, and Arnau Rios. Density dependence of the nuclear symmetry energy: A microscopic perspective. *Phys. Rev. C*, 80:045806, Oct 2009.
- [42] A. Akmal, V. R. Pandharipande, and D. G. Ravenhall. Equation of state of nucleon matter and neutron star structure. *Phys. Rev. C*, 58:1804–1828, Sep 1998.
- [43] E. Khan and J. Margueron. Determination of the density dependence of the nuclear incompressibility. *Phys. Rev. C*, 88:034319, Sep 2013.